Chapter 9
Carbon Isotope Effects in Relation to CO$_2$ Assimilation by Tree Canopies

Lucas A. Cernusak and Nerea Ubierna

Abstract The carbon atoms deposited in tree rings originate from the CO$_2$ in the atmosphere to which the tree's canopy is exposed. Thus, the first control on the stable carbon-isotope composition of tree rings is by δ^{13}C of atmospheric CO$_2$. There has been an inter-annual trend of decreasing δ^{13}C of atmospheric CO$_2$ over the past two centuries as a result of combustion of fossil fuels and land-use change. Atmospheric CO$_2$ is, for the most part, well mixed, but the sub-canopy air space can become depleted in ^{13}C due to inputs from soil and plant respiration when turbulent exchange with the troposphere is hindered, for example by a high leaf area index at night. This is less likely to occur during daytime when turbulence is higher and photosynthesis takes place. Discrimination against ^{13}C (Δ^{13}C) occurs upon assimilation of atmospheric CO$_2$ by C$_3$ photosynthesis. Trees using the C$_3$ photosynthetic pathway comprise the overwhelming majority of all trees. The primary control on the extent of discrimination during C$_3$ photosynthesis is the drawdown in CO$_2$ concentration from the air outside the leaf to the site of carboxylation in the chloroplast. Part of this drawdown is captured by c_i/c_a, that is, the ratio of intercellular to ambient CO$_2$ concentrations. The c_i/c_a represents the balance between the CO$_2$ supply by stomata and its demand by photosynthesis. It can be related to water-use efficiency, the amount of CO$_2$ taken up by photosynthesis for a given amount of water loss to the atmosphere, assuming a given evaporative demand. To predict time-averaged c_i/c_a from wood Δ^{13}C, a simplified, linear model can be employed. In this linear model, the slope is determined by $\bar{b}$, the effective enzymatic discrimination. The value of $\bar{b}$ can be estimated by comparing wood Δ^{13}C to representative measurements of c_i/c_a. The $\bar{b}$ was originally estimated from observations of leaf tissue to have a value of 27‰. We compiled data for woody stem tissue here, and our analysis suggests that a lower $\bar{b}$ should be used in the simplified model for wood ($\bar{b} = 25.5$‰) than for leaves ($\bar{b} = 27$‰). This is also consistent with widespread observations that woody tissues are enriched in ^{13}C compared to leaves.

L. A. Cernusak (✉)
College of Science and Engineering, James Cook University, Cairns, QLD 4878, Australia
e-mail: lucas.cernusak@jcu.edu.au

N. Ubierna
The Australian National University, Canberra, ACT 0200, Australia

9.1   Introduction

The abundance of the heavier stable carbon isotope, ^{13}C, in plant material is modu-
lated both by its environment and by plant metabolism. The ratio ^{13}C/^{12}C is typically
expressed as δ^{13}C, which is the relative deviation of the ratio in the sample of interest
from that of an internationally accepted standard, Vienna Pee Dee Belemnite (Craig
1957; Coplen 2011). With respect to plant metabolism, stable isotopes have the
unique feature of integrating plant responses over time and space. Thus, they offer a
powerful tool to investigate photosynthetic processes and responses to environmental
change from the leaf to the ecosystem. In this chapter, we focus on δ^{13}C in tree rings
and how it is related to assimilation of CO_2 by the tree's canopy.

Tree rings have the potential to provide a time-structured archive of information
related to a tree's growth environment and its physiological responses to changes
in that environment (Fritts and Swetnam 1989; Briffa et al. 2004). Tree ring anal-
yses have provided an indispensable tool in efforts to understand how the terrestrial
biosphere is responding to the accelerating impacts of the Anthropocene (Saurer
et al. 2004; Peñuelas et al. 2011; Frank et al. 2015; van der Sleen et al. 2015). One
of the more tractable analyses that can be conducted on tree rings is to measure the
δ^{13}C of the wood that comprises the individual rings or sequences of rings. This
represents an integration of carbon laid down over a period of time. For annual rings,
this is taken as the course of a growing season (Chap. 14), or the full year in the
case of tropical trees without distinct non-growing seasons (Chap. 22). In the latter
case, there may also be a lack of clear annual rings. It is assumed that the majority
of carbon will have originated from canopy photosynthesis in that same time period,
although there can also be a contribution from stored carbon produced in previous
years (Monserud and Marshall 2001; Drew et al. 2009; Belmecheri et al. 2018).

The carbon isotope ratio of the photosynthate produced by a tree's canopy is deter-
mined primarily by two factors: the δ^{13}C of the atmospheric CO_2, which provides the
substrate for photosynthesis, and the discrimination against [13]C (Δ^{13}C) which takes
place during conversion of gaseous CO_2 into carbohydrates through the process of
photosynthesis. When these two factors are sufficiently understood, one can use the
measured δ^{13}C in a tree ring to make inferences about how the process of ^{13}C discrim-
ination responded to climatic and other environmental changes. Also, because the
Δ^{13}C is responsive to climate, there exists the possibility to reconstruct climate from
measured changes in Δ^{13}C once a calibration relating the two has been developed
(McCarroll and Loader 2004; Hartl-Meier et al. 2015). Perhaps the most widespread
use of tree ring analyses of δ^{13}C has been to reconstruct changes in intrinsic water-
use efficiency, the ratio of photosynthesis to stomatal conductance to water vapour,
over the course of a tree's adult life in response to climatic change, mainly rising
atmospheric CO_2 concentration (Francey and Farquhar 1982; Saurer et al. 2004;
Peñuelas et al. 2011; Frank et al. 2015; van der Sleen et al. 2015). This is possible
because there is a reliable relationship between Δ^{13}C, as recorded in plant biomass,
and the ratio of intercellular to ambient CO_2 concentrations, c_i/c_a, which in turn is
related to the intrinsic water-use efficiency (Farquhar et al. 1982a, b; Farquhar and

Richards [1984]). The latter represents an index of the amount of carbon that a tree took up by photosynthesis relative to its potential for releasing water to the atmosphere through transpiration (see Chap. 17). If the atmospheric vapour pressure deficit is known, then the intrinsic water use efficiency can be converted to an actual water use efficiency in terms of molar or mass units of water exchanged for carbon. More detailed physiological conclusions can be drawn when the $\delta^{13}C$ values are combined with $\delta^{18}O$ from the same sample (e.g. Chap. 16).

9.2   The $\delta^{13}C$ of Atmospheric CO$_2$

Prior to the industrial revolution, the $\delta^{13}C$ of atmospheric CO$_2$ fluctuated between about -7.5 and $-6.2‰$ for the previous 160,000 years (Fig. 9.1). These data are based on analysis of air that was trapped in ice cores. The onset of industrial activity saw increasing combustion of fossil fuels, made up of plant carbon deposited in geological reservoirs millions of years ago. This fossil carbon carries a $\delta^{13}C$ signature reflecting photosynthetic discrimination against ^{13}C, and has $\delta^{13}C$ roughly similar to C$_3$ plants of today, with global emissions having a weighted mean $\delta^{13}C$ of ~$-28‰$ in recent decades (Andres et al. [1996], [2000]). The CO$_2$ released from combustion of fossil fuels associated with the industrial revolution began to accumulate in the atmosphere after the mid-18th Century, and the atmospheric CO$_2$ concentration increased from a pre-industrial value of ~280 μmol mol^{-1} to ~407 μmol mol^{-1} in 2018. Associated with this, the $\delta^{13}C$ of atmospheric CO$_2$ began to decline (Fig. 9.1).From about 1960 onwards, it declined at a steeper rate, reaching $-8.5‰$ in 2018 (Table 9.1). This was associated with an acceleration in the rate of fossil fuel emissions around this time (Andres et al. [2012]). The depletion in ^{13}C of atmospheric CO$_2$ caused by the addition of CO$_2$ from combustion of fossil fuels during the industrial period is referred to as the ^{13}C Suess Effect (Keeling [1979]), by analogy to the decrease in ^{14}C of CO$_2$ discovered by Hans Suess ([1955]).

Both the atmospheric CO$_2$ concentration and its $\delta^{13}C$ show an intra-annual, or seasonal, cycle associated with photosynthesis in summer months and respiration in winter months in the northern hemisphere (Fig. 9.1). This seasonal cycle is most pronounced at high latitudes in the northern hemisphere, less pronounced at tropical latitudes, and essentially absent at high latitudes of the southern hemisphere, where there is very little land mass and therefore little terrestrial productivity (Keeling et al. [2005]). In addition to this latitudinal and hemispheric gradient in the seasonal cycle of CO$_2$ concentration and isotopic composition, there is also an interhemispheric gradient in seasonally adjusted values for these variables; that is, their values when the seasonal cycle has been statistically removed. The interhemispheric gradient is such that the atmospheric CO$_2$ concentration is higher in the northern than in the southern hemisphere, and this concentration difference has been increasing since direct atmospheric measurements commenced around 1960 (Keeling et al. [2011]). It is accompanied by a difference in seasonally adjusted atmospheric $\delta^{13}C$ of CO$_2$ on the order of 0.1‰, in which $\delta^{13}C$ of CO$_2$ in the northern hemisphere is more negative
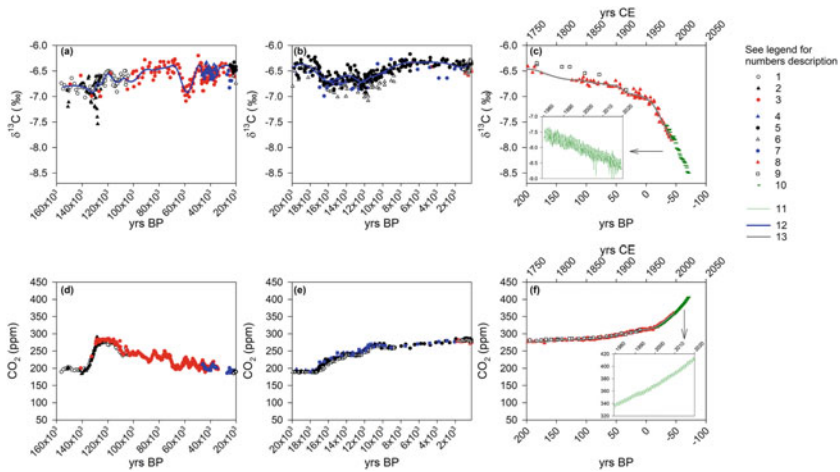
Fig. 9.1 The stable isotope composition (δ^{13}C, panels **a** to **c**) and CO_2 concentration ([CO_2], panels **d** to **f**) of atmospheric CO_2 over the last ~160,000 years. Time is in years before present (yrs BP), where zero corresponds to the year 1950 of the current era (CE). In panels **c** and **f** both yrs BP and CE scales are presented. Data are from studies reporting both δ^{13}C and [CO_2] in either ice cores or atmospheric air samples. For each data series the information presented next corresponds to the number in the legend—*symbol*—time span (Kyrs BP or CE)—sample origin (ice core drilling location or atmospheric station)—reference. Data series: 1—*White circles*—156.3 to 104.3 Kyrs BP—European Project for IceCoring in Antarctica (EPICA) Dome C (EDC) and Talos Dome— Schneider et al. (2013); 2—*Black triangles*—151.7 to 125.2 Kyrs BP—EDC—Lourantou et al. (2010); 3—*Red circles*—149.5 to 1.5 Kyrs BP – EDC, Talos Dome and EPICA Dronning Maud Land (EDML) – Eggleston et al. (2016); 4—*Blue triangles*—46.4 to 10.9 Kyrs BP—Taylor Dome— Bauska et al. (2016, 2018); 5—*Black circles*—24.4 to 0.5 Kyrs BP—EDC and Talos Dome—Schmitt et al. (2012); 6—*White triangles*—22.0 to 8.8 Kyrs BP—EDC—Lourantou et al. (2010); 7—*Blue circles*—27.1 to 1.3 Kyrs BP—Taylor Dome—Indermuhle et al. (1999); Smith et al. (1999); 8—*Red triangles*—1.8 to −0.04 Kyrs BP—Law Dome—Rubino et al. (2019); 9—*White squares*—1.2 to −0.01 Kyrs BP—WAIS Divide—Bauska et al. (2015); 10 – *Green horizontal lines* – air samples at Mauna Loa and South Pole – 1960 to 2018 CE—Keeling et al. (2001, 2017), Table S3 in Supplemental Materials). Series 10 shows seasonally detrended monthly records while Series 11 (*Green line* in the inserts of panels **c** and **f**) show the seasonal trends for δ^{13}C (Keeling et al. 2001) and [CO_2] (NOAA ESRL-Global Monitoring Division) in air samples from Mauna Loa. The *Blue line* (12) is the Monte Carlo spline fitted to the δ^{13}C data in series 1, 3 and 5 by Eggleston et al. (2016). The *Grey lines* (13) are the splines fitted to Law Dome ice core records of δ^{13}C and [CO_2] by Rubino et al. (2019). Online resources: 1. https://doi.pangaea.de/10.1594/PANGAEA.817041 2. ftp://ftp.ncdc. noaa.gov/pub/data/paleo/icecore/antarctica/epica_domec/edc2010d13co2-t2.txt 3. https://doi.org/ 10.1594/PANGAEA.859209, https://doi.org/10.1594/PANGAEA.859179 4. https://www1.ncdc. noaa.gov/pub/data/paleo/icecore/antarctica/taylor/taylor2018d13co2.txt 5. https://doi.org/10.1594/ PANGAEA.772713 6. ftp://ftp.ncdc.noaa.gov/pub/data/paleo/icecore/antarctica/epica_domec/edc 2010d13co2.txt 7. ftp://ftp.ncdc.noaa.gov/pub/data/paleo/icecore/antarctica/taylor/taylor_co2-lat equat.txt 8 and 13. https://doi.org/10.25919/5bfe29ff807fb 9. ftp://ftp.ncdc.noaa.gov/pub/data/ paleo/icecore/antarctica/wais2015d13co2.txt and ftp://ftp.ncdc.noaa.gov/pub/data/paleo/icecore/ antarctica/wais2015co2.txt 10. https://scrippsco2.ucsd.edu 11. https://scrippsco2.ucsd.edu/assets/ data/atmospheric/stations/flask_isotopic/daily/daily_flask_c13_mlo.csv and ftp://aftp.cmdl.noaa. gov/products/trends/co2/co2_mm_mlo.txt 12. http://www1.ncdc.noaa.gov/pub/data/paleo/icecore/ antarctica/eggleston2016d13co2.txt. The age chronologies are: AICC2012 (Bazin et al. 2013) for series 1 and 3, EDC3_gas_a according to the 4th scenario (Loulergue et al. 2007) for series 2 and 6, LDC 2010 (Lemieux-Dudon et al. 2010) for series 5, Baggenstos et al. (2017) for series 4, and st9810 (Steig et al. 1998) for series 7

Table 9.1 Annual values for $\delta^{13}C$ (‰) and CO_2 concentration (ppm) of atmospheric CO_2 for the period 1850 to 2018. Data from 1850 to 1979 are the splines fitted by Rubino et al. (2019) to ice core records from Law Dome, Antarctica. Data from 1980 to 2018 are the average of annual records of atmospheric samples collected at Mauna Loa, Hawaii and the South Pole Observatory (Keeling et al. 2001)

Year	$\delta^{13}C$	[CO_2]	Year	$\delta^{13}C$	[CO_2]	Year	$\delta^{13}C$	[CO_2]	Year	$\delta^{13}C$	[CO_2]
1850	−6.71	285.5	1893	−6.78	293.5	1936	−6.98	308.4	1979	−7.54	334.9
1851	−6.71	285.6	1894	−6.78	293.5	1937	−6.98	309.0	1980	−7.56	337.9
1852	−6.71	285.6	1895	−6.78	293.6	1938	−6.98	309.6	1981	−7.58	339.2
1853	−6.71	285.5	1896	−6.78	293.8	1939	−6.99	310.1	1982	−7.57	340.2
1854	−6.72	285.4	1897	−6.78	294.0	1940	−6.99	310.5	1983	−7.65	341.9
1855	−6.72	285.2	1898	−6.78	294.3	1941	−6.99	311.0	1984	−7.70	343.5
1856	−6.72	285.0	1899	−6.79	294.7	1942	−7.00	311.4	1985	−7.66	344.8
1857	−6.72	284.9	1900	−6.79	295.1	1943	−7.00	311.7	1986	−7.64	346.2
1858	−6.72	285.0	1901	−6.79	295.5	1944	−7.01	311.9	1987	−7.70	348.0
1859	−6.72	285.0	1902	−6.80	296.0	1945	−7.01	311.8	1988	−7.77	350.3
1860	−6.73	285.1	1903	−6.81	296.4	1946	−7.02	311.7	1989	−7.80	351.7
1861	−6.73	285.2	1904	−6.81	296.9	1947	−7.02	311.6	1990	−7.82	353.1
1862	−6.73	285.3	1905	−6.82	297.3	1948	−7.03	311.6	1991	−7.80	354.4
1863	−6.73	285.5	1906	−6.83	297.6	1949	−7.03	311.6	1992	−7.81	355.4
1864	−6.73	285.7	1907	−6.84	297.9	1950	−7.04	311.8	1993	−7.78	356.1
1865	−6.73	286.0	1908	−6.84	298.1	1951	−7.05	312.1	1994	−7.83	357.6
1866	−6.73	286.3	1909	−6.85	298.3	1952	−7.06	312.4	1995	−7.85	359.5
1867	−6.74	286.6	1910	−6.86	298.5	1953	−7.06	312.9	1996	−7.91	361.3
1868	−6.74	287.0	1911	−6.87	298.8	1954	−7.07	313.4	1997	−7.91	362.4
1869	−6.74	287.4	1912	−6.88	299.3	1955	−7.08	313.9	1998	−8.01	365.1
1870	−6.74	287.7	1913	−6.89	299.9	1956	−7.09	314.4	1999	−8.02	366.9
1871	−6.74	288.1	1914	−6.90	300.6	1957	−7.10	314.8	2000	−8.03	368.4
1872	−6.74	288.4	1915	−6.90	301.2	1958	−7.11	315.0	2001	−8.04	369.8
1873	−6.74	288.7	1916	−6.91	301.9	1959	−7.13	315.2	2002	−8.06	371.8
1874	−6.75	288.9	1917	−6.92	302.6	1960	−7.14	315.5	2003	−8.12	374.3
1875	−6.75	289.1	1918	−6.92	303.2	1961	−7.15	316.0	2004	−8.16	376.0
1876	−6.75	289.2	1919	−6.93	303.7	1962	−7.17	316.9	2005	−8.20	378.2
1877	−6.75	289.1	1920	−6.93	304.1	1963	−7.19	317.8	2006	−8.21	380.1
1878	−6.75	289.1	1921	−6.94	304.5	1964	−7.20	318.6	2007	−8.22	382.1
1879	−6.75	289.1	1922	−6.94	304.8	1965	−7.22	319.4	2008	−8.23	384.0
1880	−6.76	289.1	1923	−6.94	304.9	1966	−7.24	320.1	2009	−8.24	385.6
1881	−6.76	289.3	1924	−6.95	305.0	1967	−7.27	321.0	2010	−8.27	387.8
1882	−6.76	289.5	1925	−6.95	305.1	1968	−7.29	321.9	2011	−8.28	389.7

(continued)

Table 9.1 (continued)

Year	$\delta^{13}C$	[CO_2]	Year	$\delta^{13}C$	[CO_2]	Year	$\delta^{13}C$	[CO_2]	Year	$\delta^{13}C$	[CO_2]
1883	−6.76	289.8	1926	−6.95	305.2	1969	−7.31	322.9	2012	−8.30	391.8
1884	−6.77	290.0	1927	−6.95	305.5	1970	−7.33	324.1	2013	−8.35	394.8
1885	−6.77	290.3	1928	−6.96	305.9	1971	−7.36	325.3	2014	−8.35	396.9
1886	−6.77	290.6	1929	−6.96	306.1	1972	−7.38	326.6	2015	−8.39	399.2
1887	−6.77	291.1	1930	−6.96	306.3	1973	−7.40	327.9	2016	−8.47	402.3
1888	−6.77	291.6	1931	−6.96	306.5	1974	−7.43	329.2	2017	−8.49	404.6
1889	−6.77	292.1	1932	−6.97	306.8	1975	−7.45	330.4	2018	−8.50	406.9
1890	−6.78	292.5	1933	−6.97	307.1	1976	−7.47	331.6			
1891	−6.78	292.9	1934	−6.97	307.4	1977	−7.49	332.7			
1892	−6.78	293.3	1935	−6.97	307.9	1978	−7.52	333.8			

than that in the southern hemisphere. These interhemispheric gradients largely reflect the greater intensity of fossil fuel emissions in the northern hemisphere compared to the southern hemisphere. However, there is also a natural gradient that can be seen if fossil fuel emissions are statistically removed; this appears to be related to oceanic transport processes (Keeling et al. 2011).

Despite these complexities, it is still true from a broader perspective that in the troposphere, the concentration of CO_2 and its $\delta^{13}C$ are generally well mixed. For example, the interhemispheric gradient in $\delta^{13}C$ of CO_2 of ~0.1‰ is of the same order of magnitude as the measurement uncertainly for $\delta^{13}C$ in wood samples. Thus, it is probably not relevant for tree ring studies. However, at the land surface, in ecosystems where vegetation canopies are dense and fluxes of carbon into and out of vegetation and soils are large, the air CO_2 concentration and $\delta^{13}C$ can become partly uncoupled from the free troposphere above. This uncoupling should be most pronounced where carbon cycling is vigorous and leaf area indices are high, such as in tropical rainforests. An example of the air CO_2 concentration and its $\delta^{13}C$ for a tropical rainforest in French Guiana is shown in Fig. 9.2. There is a notable build-up of CO_2 beneath the canopy at night, with the highest values near the forest floor fed by respiration from soils that are relatively warm and moist, and have large root biomass. The build-up of CO_2 shifts the $\delta^{13}C$ toward that of C_3 plants, because the additional CO_2 comes from respiration fuelled by carbohydrates captured in photosynthesis and decomposition of dead plant material. As a result, the $\delta^{13}C$ of atmospheric CO_2 in the forest understory can be as low as −12‰ (Buchmann et al. 1997; Pataki et al. 2003). However, such pronounced build-up of respired CO_2 is generally limited to night time conditions when there is little atmospheric turbulence and therefore less effective mixing of air beneath the canopy with that above.

Under photosynthetic conditions, when the sun shines, the land surface heats causing turbulence, and atmospheric mixing is therefore more effective. Buchmann et al. (1997) estimated that at 2 m height in a tropical rainforest the daytime $\delta^{13}C$ of CO_2 weighted by the top of canopy photosynthetically active radiation was only about 1‰ more negative than the free tropospheric value. In contrast to this relatively

Tropical rainforest: Paracou, French Guiana (leaf area index = 8)
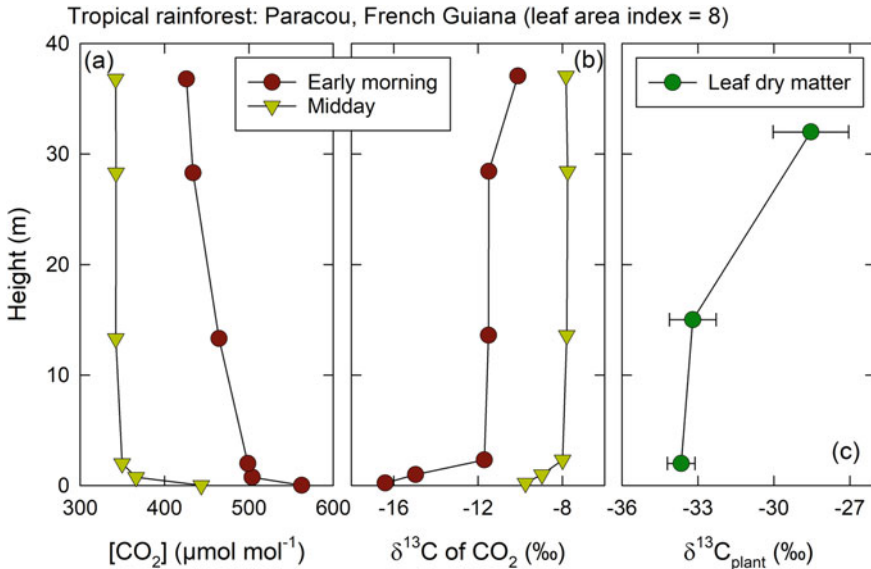
Fig. 9.2 The CO_2 concentration (**a**) and its $\delta^{13}C$ (**b**) measured in a tropical rainforest in early morning, before the onset of turbulent mixing, and at midday, when the canopy air space is typically well mixed. The more negative $\delta^{13}C$ of CO_2 in the understory is also reflected in the $\delta^{13}C$ of leaf dry matter (**c**), explaining part of the gradient in leaf dry matter $\delta^{13}C$ from top of canopy to the understory. Comparison of panels b and c shows that other factors in addition to $\delta^{13}C$ of CO_2 must be driving the reduction in $\delta^{13}C_{plant}$ from canopy top to understory, with reduction in light likely the most important of these. The figure is redrawn from Buchmann et al. (1997), using data they presented for the dry season

modest daytime shift in $\delta^{13}C$ of atmospheric CO_2 with canopy depth, the gradient in $\delta^{13}C$ of leaf biomass ($\delta^{13}C_p$) from upper canopy to understory can be up to 5‰ (Fig. 9.2c). The much steeper gradient in leaf $\delta^{13}C_p$ compared to that in daytime $\delta^{13}C$ of CO_2 suggests that physiological effects predominate in driving the changes in leaf biomass $\delta^{13}C$ (Le Roux et al. 2001; Buchmann et al. 2002; Duursma and Marshall 2006; Ubierna and Marshall 2011). These physiological effects are likely driven by the reduction in light with canopy depth. The amount of photosynthetically active radiation in the understory of a forest with leaf area index of 8, for example, can be as little as 1% of that above the canopy (Duursma and Mäkelä 2007). Such strong gradients in light result in lower chloroplastic CO_2 concentrations at top of the canopy than at depth, and therefore lower photosynthetic ^{13}C discrimination in sun than in shade foliage.

For trees that grow with their crowns in the forest canopy or in communities with lower leaf area indices, the $\delta^{13}C$ of atmospheric CO_2 that forms the source for photosynthesis can be assumed similar to that of the free troposphere (Buchmann et al. 2002). For trees with their crowns near the forest floor in communities with dense canopies, Buchmann et al. (2002) provide a relatively simple, empirical approach to estimating the daytime depletion of $\delta^{13}C$ of atmospheric CO_2 as a function of canopy

height. This is most relevant to the lowermost 2 m of the canopy air space near the forest floor.

Typically for tree ring studies, an annually averaged value for the $\delta^{13}C$ of CO_2 in the troposphere is needed. This can be compiled for years prior to 1980 based on ice core data, and for years after 1980 from flask measurements of atmospheric CO_2 that can be accessed online (https://scrippsco2.ucsd.edu/data/atmospheric_co2/sampling_stations.html), with details of the measurements described in Keeling et al. (2001). In Table 9.1, we compile annually averaged values which are updated since the values given by McCarroll and Loader (2004). The ice core $\delta^{13}C$ record was revised recently (Rubino et al. 2019), such that the value in 1850 is best estimated as ~−6.7‰, rather than about ~−6.4‰ at the time that McCarroll and Loader (2004) compiled their table. In Table 9.1, we list the spline fitted data from Rubino et al. (2019) for the years 1850 to 1979, because the directly measured ice core data are not annually resolved. For years from 1980 to 2018, we list the average of flask measurements from Mauna Loa and South Pole (Graven et al. 2017; Keeling et al. 2017). The interhemispheric gradient in $\delta^{13}C$ of CO_2 between Mauna Loa and South Pole is small, less than 0.1‰ for most years, and the continuity with the ice core record at the changeover point from 1979 to 1980 is good (Table 9.1). An alternative to using spline fitted data is to use separate regression equations for prior to 1960 and following 1960, an approach favoured by McCarroll and Loader (2004). For comparison to their values, we provide such regression equations in Fig. 9.3. Note, however, that the annual values listed in Table 9.1 are not from these regression equations, but rather from the sources described above. During preparation of this book chapter, Belmecheri and Lavergne (2020) also published a new up-to-date compilation of atmospheric CO_2 concentrations and $\delta^{13}C$ for use in tree ring studies. Although they used different datasets for their compilation than we did for Table 9.1, the two compilations agree to within 1.6 ppm for [CO_2] and 0.1‰ for $\delta^{13}C$ for individual years, with mean differences of 0.5 ppm and 0.03‰ for [CO_2] and $\delta^{13}C$, respectively.

9.3   Photosynthetic Discrimination Against ^{13}C

Once an estimate for the $\delta^{13}C$ of the air that a plant was exposed to ($\delta^{13}C_a$) has been obtained, and the $\delta^{13}C$ of plant tissue measured ($\delta^{13}C_p$), the ^{13}C discrimination of the plant tissue ($\Delta^{13}C_p$) can be calculated (Farquhar et al. 1989),

$$\Delta^{13}C_p = \frac{\delta^{13}C_a - \delta^{13}C_p}{1 + \delta^{13}C_p} \qquad (9.1a)$$

The delta values are typically expressed in per mil, which means that they will have been multiplied by 1000. When Eq. (9.1a) is scaled to per mil, the left side of the equation and the terms in the numerator of the right side will be multiplied by
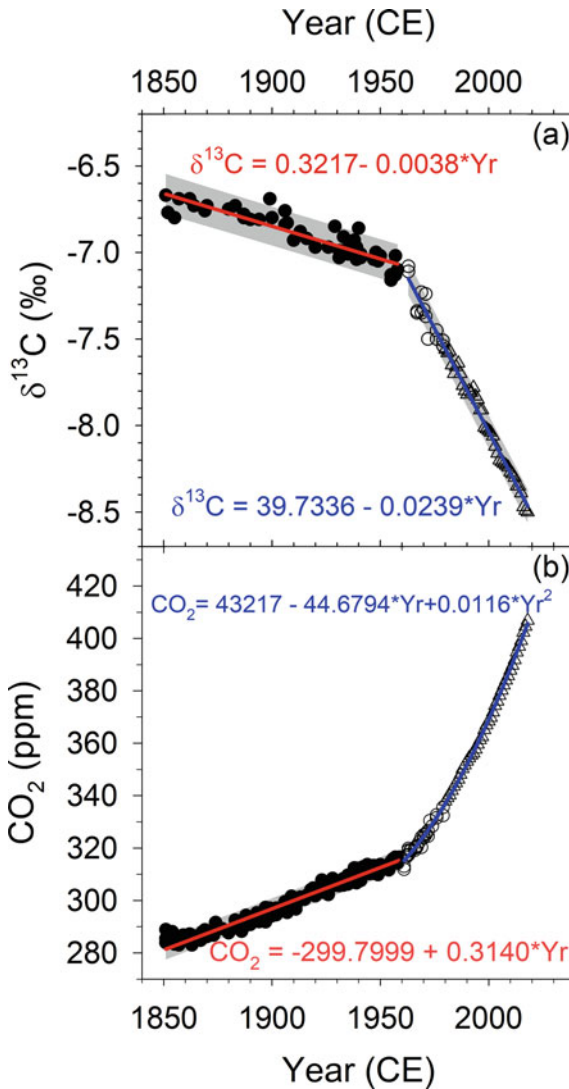
Fig. 9.3 Alternatively to values given in Table 9.1, annual $\delta^{13}C$ and CO_2 concentration can be estimated from fitted functions. In this case, two time periods are considered as distinct (McCarroll and Loader, 2004): from 1850 to 1960 (*Period 1*), and from 1961 to 2018 (*Period 2*). Data used for *Period 1* are the original ice core records from Rubino et al. (2019) (black circles in panels **a** and **b**), which differ from the spline fitted values displayed in Table 9.1. Data used for *Period 2* are a combination of ice cores (clear circles, from 1961 to 1979, Rubino et al. 2019 original values) and atmospheric CO_2 records (clear triangles, from 1980 to 2018, Keeling et al. 2001). The grey shaded areas around each fitted line represent the 95% prediction limits. Functions for $\delta^{13}C$ are: *Period 1*) $\delta^{13}C = (0.3217 \pm 0.4487) - (-0.0038 \pm 0.0002)*Year$, $R^2 = 0.83$, $P < 0.0001$, df = 51; *Period 2*) $\delta^{13}C = (39.7336 \pm 0.7971) - (0.0239 \pm 0.0004)*Year$, $R^2 = 0.99$, $P < 0.0001$, df = 51. Functions for [CO_2] are: *Period 1*) [CO_2] = (-299.7999 $\pm$ 9.8124) – (0.3140 $\pm$ 0.0051)*Year, $R^2 = 0.96$, $P < 0.0001$, df = 158; *Period 2*) [CO_2] = (43,217 $\pm$ 2120.2725) – (44.6794 $\pm$ 2.1335)*Year + (0.0116 $\pm$ 0.0005)*$Year^2$, $R^2 = 1$, $P < 0.0001$, df = 68

the factor 1000. Therefore, if the $\delta^{13}C_a$ and $\delta^{13}C_p$ are already expressed in per mil, Eq. (9.1a) will be written as,

$$\Delta^{13}C_p(\%_{00}) = \frac{\delta^{13}C_a(\%_{00}) - \delta^{13}C_p(\%_{00})}{1 + \frac{\delta^{13}C_p(\%_{00})}{1000}} \tag{9.1b}$$

Thus, the ^{13}C discrimination essentially expresses the difference between the $\delta^{13}C$ of atmospheric CO_2 and that of plant tissue, with the denominator on the right side of the equation typically increasing that value by a factor of 1.02 to 1.03.

For C_3 plants, which include the vast majority of all tree species, the $\Delta^{13}C_p$ can then be related to c_i/c_a according to the theoretical model of Farquhar et al. (1982b). In its simplest form, this model can be expressed as,

$$\Delta^{13}C_p \approx a_s + (\overline{b} - a_s)\frac{c_i}{c_a} \tag{9.2}$$

Here, a_s is the $^{13}C/^{12}C$ fractionation that takes place during diffusion of CO_2 through static air, such as in the stomatal pore. The a_s has a theoretical value of 4.4‰. The term $\overline{b}$ represents discrimination against $^{13}CO_2$ by carboxylating enzymes, mainly Rubisco. In this simplified form of the model, the term $\overline{b}$ also encompasses some other known sources of variation in $\delta^{13}C_p$, such as the diffusion resistance from the intercellular air spaces to the sites of carboxylation in the chloroplasts (Ubierna and Farquhar 2014). The value that is commonly assumed for $\overline{b}$ is 27‰. This estimate was first based on comparison of instantaneous measurements of c_i/c_a from leaf gas exchange with $\Delta^{13}C_p$ measured in leaf tissue (Farquhar et al. 1982a). Subsequent measurements of instantaneous gas exchange and leaf tissue $\delta^{13}C_p$ have also generally supported a value for $\overline{b}$ of 27‰ with respect to leaf dry matter (Farquhar et al. 1989; Cernusak et al. 2013; Cernusak 2020).

The objective for tree ring studies is often to retrieve an estimate of c_i/c_a from measurements of $\Delta^{13}C_p$. For this, Eq. (9.2) can be rearranged,

$$\frac{c_i}{c_a} \approx \frac{\Delta^{13}C_p - a_s}{\overline{b} - a_s} \tag{9.3}$$

Finally, the intrinsic water use efficiency, A/g_s, where A is net photosynthesis and g_s is stomatal conductance to water vapour, can be calculated as,

$$\frac{A}{g_s} \approx \frac{c_a\left(1 - \frac{c_i}{c_a}\right)}{1.6} \tag{9.4}$$

The factor of 1.6 in the denominator represents the ratio between the stomatal conductance to water vapour and that to CO_2. Note that Eq. (9.4) ignores both boundary layer resistance and ternary effects, and is thus a reasonable simplification of a more precise treatment (von Caemmerer and Farquhar 1981).

As noted above, Eq. (9.2) represents a simplified version of a more elaborate model for $\Delta^{13}C$ during C$_3$ photosynthesis (Farquhar et al. 1982b; Farquhar and Cernusak 2012; Busch et al. 2020),

$$\Delta^{13}C \approx \frac{1}{1-t}\left(a_b\frac{c_a-c_s}{c_a}+a_s\frac{c_s-c_i}{c_a}\right)+\frac{1+t}{1-t}\left(a_m\frac{c_i-c_c}{c_a}+b\frac{c_c}{c_a}-e\frac{\mathcal{R}_d}{A}\frac{c_c}{c_a}-f\frac{\Gamma^*}{c_a}\right)$$
$$(9.5)$$

Here, a_b is the $^{13}C/^{12}C$ fractionation during diffusion of CO$_2$ through the boundary layer (2.9‰), and a_m is that for dissolution and diffusion from the intercellular air spaces to the sites of carboxylation in the chloroplasts (1.8‰). The term b represents fractionation by Rubisco (~29‰), e is fractionation during day respiration, and f is fractionation during photorespiration. The fractionation factor assigned for e should take into account both respiratory fractionation, estimated at between 0 and 5‰ (Tcherkez et al. 2010, 2011) and any offset between $\delta^{13}C$ of respiratory substrate and the substrate currently being produced by photosynthesis (Wingate et al. 2007; Busch et al. 2020). Estimates of fractionation for photorespiration, f, range from 8 to 16‰ (Gillon and Griffiths 1997; Lanigan et al. 2008; Evans and von Caemmerer 2013). The R_d is the rate of day respiration, and Γ^* is the CO$_2$ compensation point in the absence of day respiration. The terms c_s and c_c represent the CO$_2$ concentrations at the leaf surface and at the sites of carboxylation, respectively. The term t is a ternary correction factor, defined approximately as $t\approx E/2g_c$, where E is transpiration rate and g_c is stomatal conductance to CO$_2$ (Farquhar and Cernusak 2012). For further description of the terms in Eq. (9.5), the reader is referred to Ubierna et al. (2018).

The reader will notice that the value taken for b, discrimination by Rubisco, in the more complete model, Eq. (9.5), is typically 29‰, whereas the value taken for $\bar{b}$ in the simple model, Eq. (9.2), for leaf tissue is smaller at 27‰. Below we discuss an even smaller value that should be used in the simple model for woody tissue. The difference arises because $\bar{b}$ becomes something of a catch all for several less important terms that are in Eq. (9.5), but neglected from Eq. (9.2). A hierarchical approach to removing these terms was provided by Ubierna and Farquhar (2014), from which the impacts can be explored. Interestingly, such a bottom up approach suggested that the expected value for $\bar{b}$ is actually less than 27‰, and the estimate of 27‰ likely includes developmental effects in leaf tissue $\delta^{13}C$ (Cernusak et al. 2009a; Vogado et al. 2020) and possibly other post-photoysnthetic processes (Ubierna and Farquhar 2014). The largest impact on the difference between b and $\bar{b}$ comes from the drawdown in CO$_2$ concentration between the intercellular air spaces and the sites of carboxylation in the chloroplasts. This is the effect of a finite mesophyll conductance to diffusion of CO$_2$. An additional term that could be of interest in tree ring studies is the photorespiratory fractionation, $f(\Gamma^*/c_a)$. Over large changes in atmospheric CO$_2$ concentration, there is a discernible impact on $\Delta^{13}C$ from changes in Γ^*/c_a, independent of impacts caused by changes in c_i/c_a (Schubert and Jahren 2012, 2018; Porter et al. 2019).

Equation (9.5) is thought to include all processes that impact upon discrimination against ^{13}C in photosynthetic CO$_2$ uptake by C$_3$ photosynthesis. Even so, there

are further modifications that could take place depending on the arrangement of mitochondria with respect to chloroplasts (Tholen et al. 2012; Ubierna et al. 2019), and the model does not address allocation of the products of photosynthesis, for example to starch versus export from the chloroplast (Tcherkez et al. 2004). Post photosynthetic fractionation is discussed further in Chap. 13. Equation (9.5) requires several additional parameters compared to Eq. (9.2) which are difficult to estimate retrospectively, as would be required for application to tree rings. Therefore, Eq. (9.2) represents a good compromise between mechanistic representation and tractability with respect to parameterisation. For situations where other parameters can also be measured or where accompanying datasets are available, application of the more complete model to tree rings could yield more subtle, but important, insights about past climate, leaf gas exchange, and carbon allocation dynamics within trees (Ogee et al. 2009). However, there remain challenges in understanding time integration and post-photosynthetic fractionation with respect to the $\delta^{13}C$ signal in tree rings, and these create additional complexities for knowing how and when Eq. (9.5) can be applied effectively.

9.4   Relating the $\delta^{13}C$ of Wood to Leaf Gas Exchange

As mentioned above, the value originally estimated for $\bar{b}$ in Eq. (9.2) of 27‰ was based on comparison of instantaneous measurements of c_i/c_a by leaf gas exchange with $\delta^{13}C_p$ measured in leaf tissue (Farquhar et al. 1982a). At the same time, it has long been recognized that $\delta^{13}C_p$ of wood is typically less negative than that of the leaf tissue which supplies it with photosynthate (Craig 1953; Leavitt and Long 1982; Francey et al. 1985; Leavitt and Long 1986; Badeck et al. 2005; Cernusak et al. 2009a). Differences are typically such that $\delta^{13}C_p$ of leaves is more negative than that of stem or branch wood by about 1 to 3‰. A number of hypotheses have been suggested to account for this difference, none of which are mutually exclusive (Cernusak et al. 2009a). Part of the explanation involves a depletion in leaf $\delta^{13}C_p$ that takes place during leaf expansion, such that when leaves mature, they export carbon less negative in $\delta^{13}C$ compared to their structural carbon (Evans 1983; Francey et al. 1985; Cernusak et al. 2009a; Vogado et al. 2020). There are likely additional processes during the transfer of photosynthate from chloroplasts to newly differentiating woody tissue that could contribute (Offermann et al. 2011; Gessler et al. 2014; Bögelein et al. 2019), with further discussion in Chap. 13.

Although it is difficult to define the exact processes involved, it would nevertheless seem reasonable that the value of $\bar{b}$ assigned for woody tissue in Eq. (9.2) could be less than that which would be assigned for leaf tissue. In Fig. 9.4, we compile data for 33 woody plant species in which c_i/c_a was measured by leaf gas exchange and the $\delta^{13}C_p$ was measured in both leaves and woody stem tissue. We present the data for individual plants, rather than as species averages, because in many cases treatments were imposed within a species that resulted in a within species range of c_i/c_a and $\delta^{13}C_p$. The full dataset is available in a Dryad Digital Repository (https://doi.org/10.
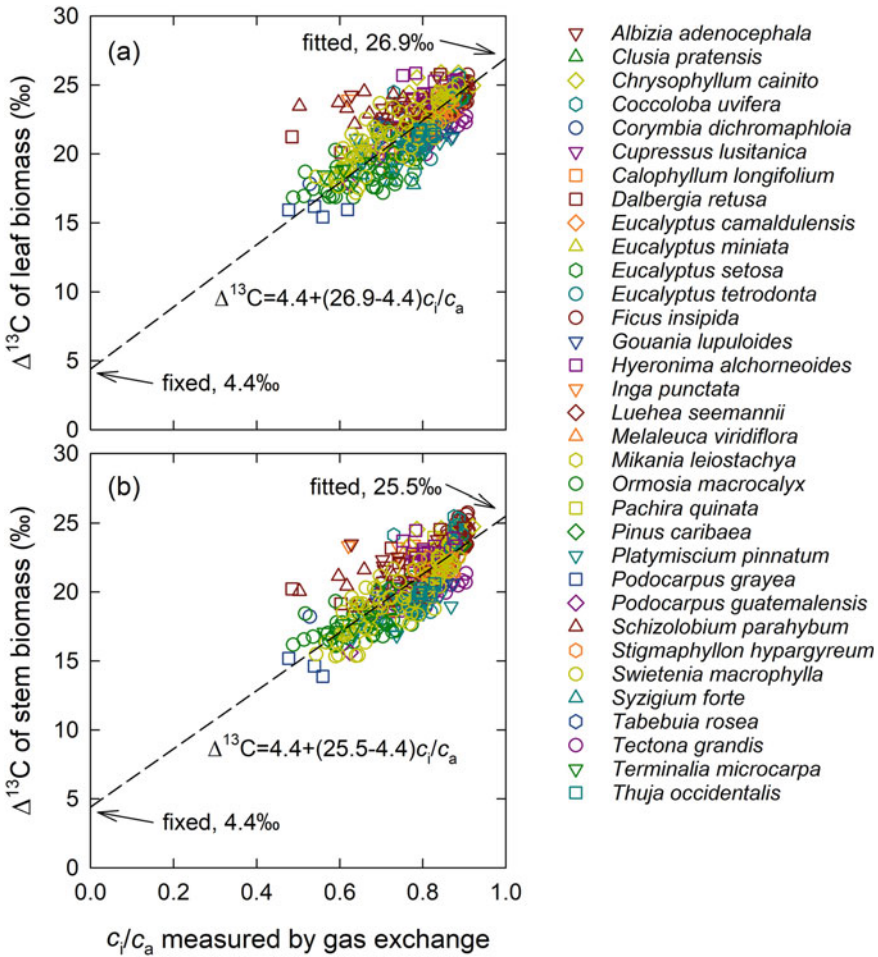
Fig. 9.4 Carbon isotope discrimination ($\Delta^{13}C$) measured in leaf biomass **a** and in stem biomass **b** plotted against the ratio of intercellular to ambient CO_2 concentrations (c_i/c_a) measured by instantaneous gas exchange in 33 woody plant species. Further details of the measurements can be found in the original publications (Cernusak et al. 2007, 2008, 2009b, 2011; Garrish et al. 2010; Cernusak 2020). The data are available in a Dryad Digital Repository (https://doi.org/10.5061/dryad.jm63xsjct). Dashed lines show regression lines fitted with the intercepts fixed at 4.4‰. The inset equations show the regression slopes applied to the simplified model of Farquhar et al. (1982b)

5061/dryad.jm63xsjct). The fitted value for $\overline{b}$ for the leaf tissue dataset, with a_s fixed at 4.4‰, was 26.9 ± 0.1‰ (coefficient ± SE; $R^2 = 0.52$, $n = 451$). This estimate is consistent with previous estimates of $\overline{b} = 27$‰ for leaf tissue. On the other hand, the estimate of $\overline{b}$ for stem tissue was 25.5 ± 0.1‰ ($R^2 = 0.63$, $n = 449$), consistent with the idea that wood is less negative in $\delta^{13}C_p$ than leaves of the same plant. Therefore, we recommend that if one aims to reconstruct c_i/c_a from leaf $\delta^{13}C_p$, a value for $\overline{b}$

of 27‰ should be used in Eq. (9.3), as is typically done. On the other hand, if one aims to reconstruct c_i/c_a from woody tissue, as is the case for tree rings, one should use a value for $\bar{b}$ of 25.5‰. The difference in c_i/c_a estimates will vary depending on the measured $\delta^{13}C_p$, but will be on the order of 0.05 in c_i/c_a. Thus, the difference is not large, but at the same time it will better align estimates of c_i/c_a from leaf and woody tissue with each other. Also, when carried through to the calculation of intrinsic water-use efficiency, the proportional change is larger, about 17% decrease in estimated A/g_s when c_i/c_a shifts from 0.7 to 0.75, for example. Note that if some parameters from Eq. (9.5) are brought in to Eq. (9.2), but Eq. (9.5) is not adopted in its entirety, then $\bar{b}$ will need to be adjusted. This would create a challenge in merging the empirically determined value of $\bar{b}$ from organic material analyses with parameters drawn from other contexts, and should be approached with caution (Vogado et al. 2020).

In order to test for species specificity in the value of $\bar{b}$ for woody tissues, we constructed a mixed effects model for wood $\Delta^{13}C$ as a function of c_i/c_a with a fixed intercept of 4.4‰; species × c_i/c_a was additionally taken as a random effect. The model thus allowed us to test for different slopes among species (indicating different $\bar{b}$ among species). The random effect was shown to be significant, with 14 out of 33 species having a slope significantly different than the overall mean slope, suggesting that $\bar{b}$ can indeed vary among species. Thus, the value for $\bar{b}$ for woody stems of 25.5‰ is a cross-species average value. However, the situation is entirely analogous to taking $\bar{b} = 27$‰ based on the average estimate for leaf tissue, as this is also a cross-species average and varies by species, as shown in Fig. 9.4a. Thus, we are suggesting moving the average from 27 to 25.5‰ for woody tissues, to correct for the overall average difference between leaf and wood $\Delta^{13}C$, but this does not address the variance around this average due to species or environment. It is an incremental step, but nonetheless seems an easy and appropriate one to take.

Often for tree-ring studies, investigators prefer to extract cellulose prior to isotopic analysis, which has both advantages and disadvantages (McCarroll and Loader 2004). The $\delta^{13}C$ of cellulose is typically less negative than that of whole wood by about 1‰ (Leavitt and Long 1982; Loader et al. 2003; Harlow et al. 2006). We recommend that if cellulose is analysed for $\delta^{13}C$, that an approximation of the offset between this and whole wood $\delta^{13}C$ be subtracted from the cellulose $\delta^{13}C$ before application of Eq. (9.3) with $\bar{b} = 25.5$‰, since this value of $\bar{b}$ was determined for whole wood.

9.5 Conclusions

In this chapter, we have reviewed the primary influences on the $\delta^{13}C$ of carbon captured by photosynthesis in C_3 plants. The first control is the $\delta^{13}C$ of atmospheric CO_2 that the plant canopy was exposed to. The $\delta^{13}C$ of atmospheric CO_2 has decreased since the onset of the industrial revolution due to release of carbon from geological reservoirs. The $\delta^{13}C$ of atmospheric CO_2 inferred from ice cores was recently revised down slightly, so that the value in 1850 is now estimated at

~-6.7‰. The mean value for 2018 was -8.5‰. The δ^{13}C of CO$_2$ beneath forest canopies can be more negative than that in the free troposphere above due to the influence of soil and plant respired CO$_2$. This decrease in δ^{13}C occurs mainly at night, and is most pronounced in forests with high leaf area indices. During daytime when photosynthesis takes place, turbulent exchange of canopy air with that in the troposphere diminishes this effect. Thus, forest respiration can reduce the δ^{13}C of the CO$_2$ that forms the source for photosynthesis of understory plants and small statured trees, but the decrease is probably not more than about 1‰ under photosynthetic conditions. A simplified model provides a means of calculating c_i/c_a, the ratio of intercellular to ambient CO$_2$ concentrations, from measurements of δ^{13}C of plant tissues and an inference of the δ^{13}C of atmospheric CO$_2$ at the time when the plant tissue was formed. The long standing observation that woody tissues are less negative in δ^{13}C than the leaves that supply them with photosynthate suggests that the coefficient relating c_i/c_a to δ^{13}C should differ for the two tissue types (see also Chap. 13). We used a dataset comprising measurements in 33 woody plant species to estimate that the coefficient $\overline{b}$ should be taken as 27‰ in the simplified model for leaf tissue, and as 25.5‰ for woody tissue, including tree rings. While the difference in estimated c_i/c_a using the two coefficients is not large, the revision will aid in aligning c_i/c_a inferred from tree rings with that which would be measured by instantaneous gas exchange.

References

Andres RJ, Marland G, Boden T, Bischof S (2000) Carbon dioxide emissions from fossil fuel consumption and cement manufacture, 1751–1991, and an estimate of their isotopic composition and latitudinal distribution. In: Schimel DS, Wigley TML (eds) The carbon cycle. Cambridge University Press, Cambridge, pp 53–62

Andres RJ, Boden TA, Breon FM, Ciais P, Davis S, Erickson D, Gregg JS, Jacobson A, Marland G, Miller J, Oda T, Olivier JGJ, Raupach MR, Rayner P, Treanton K (2012) A synthesis of carbon dioxide emissions from fossil-fuel combustion. Biogeosciences 9:1845–1871

Andres RJ, Boden TA, Marland G. 1996. Annual fossil-fuel CO$_2$ emissions: global stable carbon isotopic signature. Environmental System Science Data Infrastructure for a Virtual Ecosystem, Carbon Dioxide Information Analysis Center (CDIAC), Oak Ridge National Laboratory (ORNL), Oak Ridge, TN (United States)

Badeck FW, Tcherkez G, Nogues S, Piel C, Ghashghaie J (2005) Post-photosynthetic fractionation of stable carbon isotopes between plant organs-a widespread phenomenon. Rapid Commun Mass Spectrom 19:1381–1391

Baggenstos D, Bauska TK, Severinghaus JP, Lee JE, Schaefer H, Buizert C, Brook EJ, Shackleton S, Petrenko VV (2017) Atmospheric gas records from Taylor Glacier, Antarctica, reveal ancient ice with ages spanning the entire last glacial cycle. Clim Past 13:943–958

Bauska TK, Joos F, Mix AC, Roth R, Ahn J, Brook EJ (2015) Links between atmospheric carbon dioxide, the land carbon reservoir and climate over the past millennium. Nat Geosci 8:383–387

Bauska TK, Baggenstos D, Brook EJ, Mix AC, Marcott SA, Petrenko VV, Schaefer H, Severinghaus JP, Lee JE (2016) Carbon isotopes characterize rapid changes in atmospheric carbon dioxide during the last deglaciation. Proc Natl Acad Sci 113:3465–3470

Bauska TK, Brook EJ, Marcott SA, Baggenstos D, Shackleton S, Severinghaus JP, Petrenko VV (2018) Controls on millennial-scale atmospheric CO_2 variability during the last glacial period Geophys Res Lett 45:7731–7740

Bazin L, Landais A, Lemieux-Dudon B, Kele HTM, Veres D, Parrenin F, Martinerie P, Ritz C, Capron E, Lipenkov V, Loutre M-F, Raynaud D, Vinther B, Svensson A, Rasmussen SO, Severi M, Blunier T, Leuenberger M, Fischer H, Masson-Delmotte V, Chappellaz J, Wolff E (2013) An optimized multi-proxy, multi-site Antarctic ice and gas orbital chronology (AICC2012): 120–800 ka. Clim Past 9:1715–1731

Belmecheri S, Wright WE, Szejner P, Morino KA, Monson RK (2018) Carbon and oxygen isotope fractionations in tree rings reveal interactions between cambial phenology and seasonal climate. Plant Cell Environ 41:2758–2772

Belmecheri S, Lavergne A (2020) Compiled records of atmospheric CO_2 concentrations and stable carbon isotopes to reconstruct climate and derive plant ecophysiological indices from tree rings. Dendrochronologia 63: 125748

Bögelein R, Lehmann MM, Thomas FM (2019) Differences in carbon isotope leaf-to-phloem fractionation and mixing patterns along a vertical gradient in mature European beech and Douglas fir. New Phytol 222:1803–1815

Briffa KR, Osborn TJ, Schweingruber FH (2004) Large-scale temperature inferences from tree rings: a review. Global Planet Change 40:11–26

Buchmann N, Guehl JM, Barigah TS, Ehleringer JR (1997) Interseasonal comparison of CO_2 concentrations, isotopic composition, and carbon dynamics in an Amazonian rainforest (French Guiana). Oecologia 110:120–131

Buchmann N, Brooks JR, Ehleringer JR (2002) Predicting daytime carbon isotope ratios of atmospheric CO_2 within forest canopies. Funct Ecol 16:49–57

Busch FA, Holloway-Phillips M, Stuart-Williams H, Farquhar GD (2020) Revisiting carbon isotope discrimination in C_3 plants shows respiration rules when photosynthesis is low. Nat Plants 6:245–258

Cernusak LA (2020) Gas exchange and water-use efficiency in plant canopies. Plant Biol 22(Suppl. 1):52–67

Cernusak LA, Winter K, Aranda J, Turner BL, Marshall JD (2007) Transpiration efficiency of a tropical pioneer tree (*Ficus insipida*) in relation to soil fertility. J Exp Bot 58:3549–3566

Cernusak LA, Winter K, Aranda J, Turner BL (2008) Conifers, angiosperm trees, and lianas: growth, whole-plant water and nitrogen use efficiency, and stable isotope composition ($\delta^{13}C$ and $\delta^{18}O$) of seedlings grown in a tropical environment. Plant Physiol 148:642–659

Cernusak LA, Winter K, Turner BL (2009a) Physiological and isotopic ($\delta^{13}C$ and $\delta^{18}O$) responses of three tropical tree species to water and nutrient availability. Plant Cell Environ 32:1441–1455

Cernusak LA, Tcherkez G, Keitel C, Cornwell WK, Santiago LS, Knohl A, Barbour MM, Williams DG, Reich PB, Ellsworth DS, Dawson TE, Griffiths H, Farquhar GD, Wright IJ (2009b) Why are non-photosynthetic tissues generally ^{13}C enriched compared to leaves in C_3 plants? Review and synthesis of current hypotheses. Funct Plant Biol 36:199–213

Cernusak LA, Winter K, Martinez C, Correa E, Aranda J, Garcia M, Jaramillo C, Turner BL (2011) Responses of legume versus nonlegume tropical tree seedlings to elevated CO_2 concentration. Plant Physiol 157:372–385

Cernusak LA, Ubierna N, Winter K, Holtum JAM, Marshall JD, Farquhar GD (2013) Environmental and physiological determinants of carbon isotope discrimination in terrestrial plants. New Phytol 200:950–965

Coplen TB (2011) Guidelines and recommended terms for expression of stable-isotope-ratio and gas-ratio measurement results. Rapid Commun Mass Spectrom 25:2538–2560

Craig H (1953) The geochemistry of the stable carbon isotopes. Geochim Cosmochim Acta 3:53–92

Craig H (1957) Isotopic standards for carbon and oxygen and correction factors for mass-spectrometric analysis of carbon dioxide. Geochim Cosmochim Acta 12:133–149

Drew DM, Schulze ED, Downes GM (2009) Temporal variation in $\delta^{13}C$, wood density and microfibril angle in variously irrigated *Eucalyptus nitens*. Funct Plant Biol 36:1–10

Duursma RA, Mäkelä A (2007) Summary models for light interception and light-use efficiency of non-homogeneous canopies. Tree Physiol 27:859–870

Duursma RA, Marshall JD (2006) Vertical canopy gradients in $\delta^{13}C$ correspond with leaf nitrogen content in a mixed-species conifer forest. Trees Struct Funct 20:496–506

Eggleston S, Schmitt J, Bereiter B, Schneider R, Fischer H (2016) Evolution of the stable carbon isotope composition of atmospheric CO$_2$ over the last glacial cycle. Paleoceanography 31:434–452

Evans JR, von Caemmerer S (2013) Temperature response of carbon isotope discrimination and mesophyll conductance in tobacco. Plant Cell Environ 36:745–756

Evans JR (1983) Photosynthesis and nitrogen partitioning in leaves of *Triticum aestivum* L. and related species. PhD thesis, Australian National University, Canberra

Farquhar GD, Cernusak LA (2012) Ternary effects on the gas exchange of isotopologues of carbon dioxide. Plant Cell Environ 35:1221–1231

Farquhar GD, Richards RA (1984) Isotopic composition of plant carbon correlates with water-use efficiency in wheat genotypes. Aust J Plant Physiol 11:539–552

Farquhar GD, O'Leary MH, Berry JA (1982a) On the relationship between carbon isotope discrimination and the intercellular carbon dioxide concentration in leaves. Aust J Plant Physiol 9:121–137

Farquhar GD, Ball MC, von Caemmerer S, Roksandic Z (1982b) Effect of salinity and humidity on $\delta^{13}C$ value of halophytes- evidence for diffusional isotope fractionation determined by the ratio of intercellular/atmospheric partial pressure of CO$_2$ under different environmental conditions. Oecologia 52:121–124

Farquhar GD, Ehleringer JR, Hubick KT (1989) Carbon isotope discrimination and photosynthesis. Annu Rev Plant Physiol Plant Mol Biol 40:503–537

Francey RJ, Farquhar GD (1982) An explanation of $^{13}C/^{12}C$ variations in tree rings. Nature 297:28–31

Francey RJ, Gifford RM, Sharkey TD, Weir B (1985) Physiological influences on carbon isotope discrimination in huon pine (*Lagarostrobos franklinii*). Oecologia 66:211–218

Frank DC, Poulter B, Saurer M, Esper J, Huntingford C, Helle G, Treydte K, Zimmermann NE, Schleser GH, Ahlstrom A, Ciais P, Friedlingstein P, Levis S, Lomas M, Sitch S, Viovy N, Andreu-Hayles L, Bednarz Z, Berninger F, Boettger T, D'Alessandro CM, Daux V, Filot M, Grabner M, Gutierrez E, Haupt M, Hilasvuori E, Jungner H, Kalela-Brundin M, Krapiec M, Leuenberger M, Loader NJ, Marah H, Masson-Delmotte V, Pazdur A, Pawelczyk S, Pierre M, Planells O, Pukiene R, Reynolds-Henne CE, Rinne KT, Saracino A, Sonninen E, Stievenard M, Switsur VR, Szczepanek M, Szychowska-Krapiec E, Todaro L, Waterhouse JS, Weigl M (2015) Water-use efficiency and transpiration across European forests during the Anthropocene. Nat Clim Change 5:579–583

Fritts HC, Swetnam TW (1989) Dendroecology: a tool for evaluating variations in past and present forest environments. In: Begon M, Fitter AH, Ford ED, MacFadyen A (eds) Academic Press, Advances in Ecological Research, pp 111–188

Garrish V, Cernusak LA, Winter K, Turner BL (2010) Nitrogen to phosphorus ratio of plant biomass versus soil solution in a tropical pioneer tree, *Ficus insipida*. J Exp Bot 61:3735–3748

Gessler A, Ferrio JP, Hommel R, Treydte K, Werner RA, Monson RK (2014) Stable isotopes in tree rings: towards a mechanistic understanding of isotope fractionation and mixing processes from the leaves to the wood. Tree Physiol 34:796–818

Gillon JS, Griffiths H (1997) The influence of (photo)respiration on carbon isotope discrimination in plants. Plant Cell Environ 20:1217–1230

Graven H, Allison CE, Etheridge DM, Hammer S, Keeling RF, Levin I, Meijer HAJ, Rubino M, Tans PP, Trudinger CM, Vaughn BH, White JWC (2017) Compiled records of carbon isotopes in atmospheric CO$_2$ for historical simulations in CMIP6. Geosci Model Dev 10:4405–4417

Harlow BA, Marshall JD, Robinson AP (2006) A multi-species comparison of $\delta^{13}C$ from whole wood, extractive-free wood and holocellulose. Tree Physiol 26:767–774

Hartl-Meier C, Zang C, Buntgen U, Esper J, Rothe A, Gottlein A, Dirnback T, Treydte K (2015) Uniform climate sensitivity in tree-ring stable isotopes across species and sites in a mid-latitude temperate forest. Tree Physiol 35:4–15

Indermuhle A, Stocker TF, Joos F, Fischer H, Smith HJ, Wahlen M, Deck B, Mastroianni D, Tschumi J, Blunier T, Meyer R, Stauffer B (1999) Holocene carbon-cycle dynamics based on CO_2 trapped in ice at Taylor Dome, Antarctica. Nature 398:121–126

Keeling CD (1979) The Suess effect: [13]Carbon-[14]Carbon interrelations. Environ Int 2:229–300

Keeling CD, Piper SC, Whorf TP, Keeling RF (2011) Evolution of natural and anthropogenic fluxes of atmospheric CO_2 from 1957 to 2003. Tellus B 63:1–22

Keeling RF, Graven HD, Welp LR, Resplandy L, Bi J, Piper SC, Sun Y, Bollenbacher A, Meijer HAJ (2017) Atmospheric evidence for a global secular increase in carbon isotopic discrimination of land photosynthesis. Proc Natl Acad Sci USA 114:10361–10366

Keeling CD, Piper SC, Bacastow RB, Wahlen M, Whorf TP, Heimann M, Meijer HA (2001) Exchanges of atmospheric CO_2 and $^{13}CO_2$ with the terrestrial biosphere and oceans from 1978 to 2000. I. Global aspects, SIO Reference Series, No. 01-06: Scripps Institution of Oceanography, San Diego

Keeling CD, Piper SC, Bacastow RB, Wahlen M, Whorf TP, Heimann M, Meijer HA (2005) Atmospheric CO_2 and $^{13}CO_2$ exchange with the terrestrial biosphere and oceans from 1978 to 2000: observations and carbon cycle implications. In: Baldwin IT, Caldwell MM, Heldmaier G, Jackson RB, Lange OL, Mooney HA, Schulze ED, Sommer U, Ehleringer JR, Denise Dearing M, Cerling TE (eds) A history of atmospheric CO_2 and its effects on plants, animals, and ecosystems. Springer, New York, pp 83–113

Lanigan GJ, Betson N, Griffiths H, Seibt U (2008) Carbon isotope fractionation during photorespiration and carboxylation in *Senecio*. Plant Physiol 148:2013–2020

Le Roux X, Bariac T, Sinoquet H, Genty B, Piel C, Mariotti A, Girardin C, Richard P (2001) Spatial distribution of leaf water-use efficiency and carbon isotope discrimination within an isolated tree crown. Plant Cell Environ 24:1021–1032

Leavitt SW, Long A (1982) Evidence for $^{13}C/^{12}C$ fractionation between tree leaves and wood. Nature 298:742–744

Leavitt SW, Long A (1986) Stable-carbon isotope variability in tree foliage and wood. Ecology 67:1002–1010

Lemieux-Dudon B, Blayo E, Petit J-R, Waelbroeck C, Svensson A, Ritz C, Barnola J-M, Narcisi BM, Parrenin F (2010) Consistent dating for Antarctic and Greenland ice cores. Quatern Sci Rev 29:8–20

Loader NJ, Robertson I, McCarroll D (2003) Comparison of stable carbon isotope ratios in the whole wood, cellulose and lignin of oak tree-rings. Palaeogeogr Palaeoclimatol Palaeoecol 196:395–407

Loulergue L, Parrenin F, Blunier T, Barnola J-M, Spahni R, Schilt A, Raisbeck G, Chappellaz J (2007) New constraints on the gas age-ice age difference along the EPICA ice cores, 0–50 kyr. Clim Past 3:527–540

Lourantou A, Chappellaz J, Barnola JM, Masson-Delmotte V, Raynaud D (2010) Changes in atmospheric CO_2 and its carbon isotopic ratio during the penultimate deglaciation. Quatern Sci Rev 29:1983–1992

McCarroll D, Loader NJ (2004) Stable isotopes in tree rings. Quatern Sci Rev 23:771–801

Monserud RA, Marshall JD (2001) Time-series analysis of $\delta^{13}C$ from tree rings 1: time trends and autocorrelations. Tree Physiol 21:1087–1102

Offermann C, Ferrio JP, Holst J, Grote R, Siegwolf R, Kayler Z, Gessler A (2011) The long way down-are carbon and oxygen isotope signals in the tree ring uncoupled from canopy physiological processes? Tree Physiol 31:1088–1102

Ogee J, Barbour MM, Wingate L, Bert D, Bosc A, Stievenard M, Lambrot C, Pierre M, Bariac T, Loustau D, Dewar RC (2009) A single-substrate model to interpret intra-annual stable isotope signals in tree-ring cellulose. Plant Cell Environ 32:1071–1090

Pataki DE, Ehleringer JR, Flanagan LB, Yakir D, Bowling DR, Still CJ, Buchmann N, Kaplan JO, Berry JA (2003) The application and interpretation of Keeling plots in terrestrial carbon cycle research. Global Biogeochem Cycles 17:15

Peñuelas J, Canadell JG, Ogaya R (2011) Increased water-use efficiency during the 20th century did not translate into enhanced tree growth. Glob Ecol Biogeogr 20:597–608

Porter AS, Gerald CEF, Yiotis C, Montanez IP, McElwain JC (2019) Testing the accuracy of new paleoatmospheric CO$_2$ proxies based on plant stable carbon isotopic composition and stomatal traits in a range of simulated paleoatmospheric O$_2$:CO$_2$ ratios. Geochim Cosmochim Acta 259:69–90

Rubino M, Etheridge DM, Thornton DP, Howden R, Allison CE, Francey RJ, Langenfelds RL, Steele LP, Trudinger CM, Spencer DA, Curran MAJ, van Ommen TD, Smith AM (2019) Revised records of atmospheric trace gases CO$_2$, CH$_4$, N$_2$O, and δ^{13}C-CO$_2$ over the last 2000 years from Law Dome, Antarctica. Earth Syst Sci Data 11:473–492

Saurer M, Siegwolf RTW, Schweingruber FH (2004) Carbon isotope discrimination indicates improving water-use efficiency of trees in northern Eurasia over the last 100 years. Glob Change Biol 10:2109–2120

Schmitt J, Schneider R, Elsig J, Leuenberger D, Lourantou A, Chappellaz J, Köhler P, Joos F, Stocker TF, Leuenberger M, Fischer H (2012) Carbon isotope constraints on the deglacial CO$_2$ rise from ice cores. Science 336:711–714

Schneider R, Schmitt J, Köhler P, Joos F, Fischer H (2013) A reconstruction of atmospheric carbon dioxide and its stable carbon isotopic composition from the penultimate glacial maximum to the last glacial inception. Clim Past 9:2507–2523

Schubert BA, Jahren AH (2012) The effect of atmospheric CO$_2$ concentration on carbon isotope fractionation in C$_3$ land plants. Geochim Cosmochim Acta 96:29–43

Schubert BA, Jahren AH (2018) Incorporating the effects of photorespiration into terrestrial paleoclimate reconstruction. Earth Sci Rev 177:637–642

Smith HJ, Fischer H, Mastroianni D, Deck B, Wahlen M (1999) Dual modes of the carbon cycle since the Last Glacial Maximum. Nature 400:248–250

Steig EJ, Brook EJ, White JWC, Sucher CM, Bender ML, Lehman SJ, Morse DL, Waddington ED, Clow GD (1998) Synchronous climate changes in Antarctica and the North Atlantic. Science 282:92–95

Suess HE (1955) Radiocarbon concentration in modern wood. Science 122:415

Tcherkez G, Farquhar G, Badeck F, Ghashghaie J (2004) Theoretical considerations about carbon isotope distribution in glucose of C$_3$ plants. Funct Plant Biol 31:857–877

Tcherkez G, Schaufele R, Nogues S, Piel C, Boom A, Lanigan G, Barbaroux C, Mata C, Elhani S, Hemming D, Maguas C, Yakir D, Badeck FW, Griffiths H, Schnyder H, Ghashghaie J (2010) On the ^{13}C/^{12}C isotopic signal of day and night respiration at the mesocosm level. Plant Cell Environ 33:900–913

Tcherkez G, Mauve C, Lamothe M, Le Bras C, Grapin A (2011) The ^{13}C/^{12}C isotopic signal of day-respired CO$_2$ in variegated leaves of *Pelargonium* x *hortorum*. Plant Cell Environ 34:270–283

Tholen D, Ethier G, Genty B, Pepin S, Zhu XG (2012) Variable mesophyll conductance revisited: theoretical background and experimental implications. Plant Cell Environ 35:2087–2103

Ubierna N, Farquhar GD (2014) Advances in measurements and models of photosynthetic carbon isotope discrimination in C$_3$ plants. Plant Cell Environ 37:1494–1498

Ubierna N, Marshall JD (2011) Vertical and seasonal variation in the δ^{13}C of leaf-respired CO$_2$ in a mixed conifer forest. Tree Physiol 31:414–427

Ubierna N, Cernusak LA, Holloway-Phillips M, Busch FA, Cousins AB, Farquhar GD (2019) Critical review: incorporating the arrangement of mitochondria and chloroplasts into models of photosynthesis and carbon isotope discrimination. Photosynth Res 141:5–31

Ubierna N, Holloway-Phillips MM, Farquhar GD (2018) Using stable carbon isotopes to study C$_3$ and C$_4$ photosynthesis: models and calculations. In: Covshoff S (ed) Photosynthesis: methods and protocols. Springer, New York, pp 155–196

van der Sleen P, Groenendijk P, Vlam M, Anten NPR, Boom A, Bongers F, Pons TL, Terburg G, Zuidema PA (2015) No growth stimulation of tropical trees by 150 years of CO_2 fertilization but water-use efciency increased. Nat Geosci 8:24–28

Vogado NO, Winter K, Ubierna N, Farquhar GD, Cernusak LA (2020) Directional change in leaf dry matter $\delta^{13}C$ during leaf development is widespread in C_3 plants. Annals Botany 126:981–990

von Caemmerer S, Farquhar GD (1981) Some relationships between the biochemistry of photosynthesis and the gas exchange of leaves. Planta 153:376–387

Wingate L, Seibt U, Moncrieff JB, Jarvis PG, Lloyd J (2007) Variations in ^{13}C discrimination during CO_2 exchange by *Picea sitchensis* branches in the field. Plant Cell Environ 30:600–616